


Peierls versus Holstein models for describing electron-phonon coupling in perovskitesYau-Chuen Yam , Mirko M. Moeller, George A. Sawatzky, and Mona Berciu*Department of Physics and Astronomy, University of British Columbia, Vancouver, British Columbia, Canada V6T 1Z1 and Stewart Blusson Quantum Matter Institute, University of British Columbia, Vancouver, British Columbia, Canada V6T 1Z4*

(Received 14 July 2020; revised 4 December 2020; accepted 7 December 2020; published 21 December 2020)

We use the momentum average approximation together with perturbative approaches, in the appropriate limits, to study the single polaron physics on a perovskite lattice inspired by BaBiO₃. We investigate electron-phonon coupling of the Peierls type whereby the motion of ions modulates the values of the hopping integrals between sites and show that it cannot be mapped onto the simpler one-band Holstein model in the whole parameter space. This is because the dispersion of the Peierls polaron has sharp transitions where the ground-state momentum jumps between high-symmetry points in the Brillouin zone, whereas the Holstein polaron always has the same ground-state momentum. These results imply that careful consideration is required to choose the appropriate model for carrier-lattice coupling in such complex lattices.

DOI: [10.1103/PhysRevB.102.235145](https://doi.org/10.1103/PhysRevB.102.235145)**I. INTRODUCTION**

Materials with perovskite structure ABO₃ are known to have a wide variety of extraordinary properties, ranging from unconventional high-temperature superconductivity in cuprates [1–4], to an unusual metal-to-insulator transition in rare-earth nickelates [5], to colossal magnetoresistance in manganites [6,7], to multiferroic behavior [8], among others. Many of these properties are believed to arise from the interplay of charge, spin, orbital, and lattice degrees of freedom and of their various interactions. A full detailed treatment of all this complexity is still unfeasible, resulting in the urgent need to identify simpler but useful models. For instance, is it ever necessary to consider the full multiplet structure for rare earths with partially filled shells, or does it suffice to include explicitly only one/few of them, with a simplified description for correlations? One well-known example where this kind of question is relevant is the cuprates, where most models only consider the $3d_{x^2-y^2}$ orbital for Cu [9–11]. Even more basic is the question of which of the constituent elements need to be included in the modeling. To continue with the example of the CuO₂ layer, even though it is well known that the doped holes are mostly on the anions, most models do not explicitly include them. Another example are the rare-earth nickelates, where only recently it has become clear how essential it is to include the oxygen ions in the model [12,13]. Of course, answers will vary from one material to another, but it is important to ask such questions and to understand when certain approximations may be valid and when they are certainly not.

In this work, we focus on the modeling of the electron-phonon coupling. To keep the discussion specific, from now on we will use the perovskite BaBiO₃ as our inspiration, although much of the following discussion applies to other perovskites as well. BaBiO₃ is a good choice because (i) it has no complications from strong correlations and/or spin-orbit coupling (for reasons detailed in the next section), and (ii) the

electron-phonon coupling is believed to be strong in this material, and in fact K-doped BaBiO₃ has a record high (at ambient pressure) $T_C \approx 35$ K for a superconductor with a phonon glue. The reason for this high value of T_C is not yet settled: Conventional density functional theory (DFT) results predict a much too weak coupling [14–19], although a more local molecularlike description of the electronic structure yields a substantial electron-phonon coupling [20].

However, it is not just the strength of the coupling that is still controversial but also its very form. This issue is directly linked to the one we referred to above, of how to model the crystal itself. Early work on BaBiO₃ assumed that the O $2p$ orbitals are full and that therefore only the Bi $6s$ orbitals are valence orbitals, because conventional counting gives Bi⁴⁺ with $6s^1$ electronic structure in the undoped parent compound. A naive, purely electronic model would therefore predict a metallic ground state, with a half-filled valence band described by tight-binding hopping t_{ss} between neighbor Bi sites.

This, however, is inconsistent with the experimental observation of an insulating ground state, with alternating Bi sites surrounded by expanded and collapsed O octahedra, respectively. This phenomenology can be accounted for by adding electron-phonon coupling to the model. The lattice distortion is provided by displacements of the O ions along their Bi-O-Bi bond. This makes sense not just because it is consistent with the experimental observation but also because O is the lightest ion and thus the most mobile one.

The assumptions that the valence electrons are on Bi while the phonons are on O, essentially fix the form of the possible electron-phonon coupling: Charge fluctuations on the Bi are associated with “breathing-mode”-like distortions of the O octahedra. One drives the other through Coulomb interactions, resulting in an undoped insulating ground state with alternating Bi³⁺/Bi⁵⁺ surrounded by expanded/collapsed octahedra, respectively. This so-called Rice-Sneddon electron-phonon

coupling model was extensively used to investigate the formation and properties of polarons and bipolarons in BaBiO₃ [21–24]. Subsequently, it was shown to map exactly onto a generalized Holstein model [25]. This has one effective (symmetrical) optical boson mode per octahedron, and a Holstein-like coupling g_{ij} between the density of electrons \hat{n}_i at Bi site i and the distortion $b_j^\dagger + b_j$ associated with this symmetric phonon of the octahedron surrounding the Bi site j , where g_{ij} decreases very fast with the distance $\vec{R}_i - \vec{R}_j$. Thus, to very good accuracy, the Rice-Sneddon model is equivalent to a standard Holstein model [26] with $g_{ij} = \delta_{ij}g$, and indeed this was then used to study the optical properties of BaBiO₃ and the metal-insulator transition in hole-doped BaBiO₃ [27].

Generically, electron-phonon coupling arises not just from the modulation of the electron's onsite energy like described by the Rice-Sneddon and Holstein models (from now on, for simplicity, we will only list the Holstein coupling as the representative of this class of models). It also arises because lattice distortions modulate the hopping of the electron, i.e., its kinetic energy, as originally noted by Barisic *et al.* [28]. However, we emphasize that with the assumptions that the valence electrons are on Bi while the phonons are on O, we do not expect this latter type of electron-phonon coupling to be important. Naively, one could say that because the Bi ions are fixed, there cannot be any modulation of the t_{ss} between neighboring Bi. Of course, in reality the hopping proceeds through the ligand O site, and so $t_{ss} \propto t_{sp}t_{ps}/\Delta$, where t_{sp} and t_{ps} are the hoppings between the first Bi and the ligand O, and the ligand O and the second Bi, respectively, while Δ is the charge transfer energy. Both t_{sp} and t_{ps} are modulated by the displacement of the O, however to first order these modulations cancel each other because increase of the Bi-O bond length implies a decrease of the O-Bi bond length and vice versa.

Thus, to the extent that a perovskite ABO₃ is well modelled in terms of valence orbitals on the B sites and optical phonons on the O sites, the dominant electron-phonon coupling must be of Holstein type (or the more sophisticated, but essentially equivalent, Rice-Sneddon type). This model becomes very accurate in the limit where the ratio $t_{sp}/\Delta \rightarrow 0$, as this is the condition for the O bands to be placed well below the Fermi energy (in the electron picture) and therefore be completely full.

In many (arguably most) perovskites, this ratio is not extremely small. Instead, typically there is significant hybridization between the B site and the ligand O, meaning that at least the $O2p_\sigma$ ligand orbital must be included into the set of valence orbitals, thus turning the prior one-band model into a many-band model. In particular, for BaBiO₃, recent DFT results from Foyevtsova *et al.* [29] and Khazraie *et al.* [30] have highlighted this strong hybridization between O and Bi which gives rise to the bond-disproportionated state where holes reside on the O sites in “molecularlike” orbitals.

The addition of the $O2p_\sigma$ ligand orbital in the set of valence orbitals is easy to account for, so far as the electronic component of the model is concerned. The minimal hopping Hamiltonian is now described by t_{sp} hopping between neighbor O and Bi sites, and t_{pp} hopping between neighbor O sites (for more details, see next section) and is supplemented by a

charge transfer energy Δ characterizing the energy difference between the two sets of orbitals. Of course, onsite repulsion should also be included if correlations are important, but this is not the case for BaBiO₃.

However, the explicit inclusion of the O orbitals significantly complicates the description of the electron-phonon coupling. The Holstein coupling described above is still expected to be present but is now supplemented by the second type of coupling which modulates both the t_{sp} and t_{pp} hoppings as O ions move. For brevity, we call this the Peierls coupling, although as already mentioned, it was first proposed by Barisic *et al.* [28] and was then used with great success to study polyacetylene within the Su-Schrieffer-Heeger model [31,32].

This complication of having both Holstein and Peierls electron-phonon coupling would be significantly mitigated if it could be shown that the Peierls coupling [28,31,32] can also be effectively reduced to a Holstein-like coupling. In that case, electron-phonon coupling in perovskites would be well described by a Holstein model, with a coupling strength g that accounts for both components.

In this work, we consider precisely this question of whether the Peierls [28,31,32] and Holstein models are equivalent. We are unable to provide accurate results in the physically relevant limit of half filling, i.e., when there is one hole per unit cell. This is because computational methods are still unable to deal with 3D lattices and quantum phonons; the current state of the art is a rather small 2D Lieb lattice cluster, see Ref. [33]. On the other hand, we do have access to accurate approximations in the single carrier limit. Hence, we consider the extreme case when there is a single hole in the entire system (effectively zero carrier concentration, for an infinite lattice), because here we can study the properties of the resulting polaron sufficiently accurately to draw unequivocal conclusions. Moreover, we investigate the behavior of our model in the wider parameter space, including regions that are far from where BaBiO₃ is expected to be located. This is partially due to technical reasons, as the variational approximation that we employ becomes more accurate for phonon frequencies comparable to, or larger, than the electronic bandwidth. As we show, the behavior of interest to us evolves smoothly with decreasing phonon frequencies, so some inferences can be made about what happens in the adiabatic limit. Nevertheless, it is important to find other methods that are reliable in this limit to separately verify our conclusions.

A second reason to study models with relatively narrow bandwidths is the concerted effort in modern condensed matter physics to develop so-called “flat-band” materials like twisted graphene or ordered impurity-based midgap bands in semiconductors or insulators. In such materials, the effective bandwidths can be comparable to or smaller than the phonon frequencies, and our results would be directly relevant to them.

Our results demonstrate that in certain regions of the parameter space, the Peierls model [28,31,32] on a perovskite lattice exhibits single polaron behavior that is impossible to reproduce with a Holstein model. Specifically, as the electron-phonon coupling is increased, the polaron dispersion changes its shape such that the ground-state momentum switches from its free-carrier value to another high-symmetry point in the

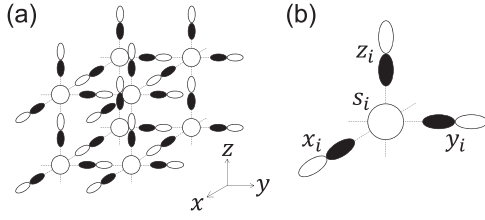


FIG. 1. (a) Sketch of the model for an infinite 3D lattice, showing s orbitals at the B sites, and the ligand $2p$ orbitals at the O sites. The A sites are ignored. (b) Our choice for the unit cell i has an s orbital labeled by s_i and three $2p$ orbitals labeled x_i , y_i , and z_i along the three ligand bonds.

Brillouin zone. Such discontinuous, sharp transitions are impossible to occur in the ground-state properties of a Holstein polaron [34]. Based on this result, we conclude that the Peierls model cannot always be replaced with a Holstein model when studying a perovskite system.

This being said, it is important to emphasize the caveat that our study is in the single-polaron limit. It is possible that at finite carrier concentration, the mapping between Peierls [28,31,32] and Holstein couplings might be valid for some other reasons—however, this has to be explicitly verified. To the best of our knowledge, there is no work addressing this question. We also emphasize that there are regions of the parameter space (including the region where BaBiO_3 is believed to be located) where the single polaron ground-state momentum equals the free-carrier value, and therefore a Holstein model may be sufficient to mimic the polaron behavior for a correct choice of effective parameters. (This statement still remains to be verified at half filling).

The key result of our study is that equivalence between Peierls and Holstein models is not guaranteed for perovskite materials, therefore one must either explicitly include the Peierls coupling [28,31,32] in the model, or one must do detailed work to justify the use of a Holstein model as a reasonable description of the electron-phonon coupling for that specific material (set of parameters).

The paper is organized as follows: In Sec. II we introduce our model, in Sec. III we describe the various methods we used to study it, and in Sec. IV we present the results. Section V contains the discussion and conclusions. Technical details are relegated to the appendices.

II. MODEL

We use the following approximations to model the generic perovskite ABO_3 :

(i) Sites A are taken to be irrelevant for the physics of interest to us and are ignored. Physically, this implies that electronic bands with dominant A character are lying well below and/or well above the Fermi energy. For BaBiO_3 , which is our main inspiration, this is a good approximation. It reduces the lattice of interest from a full perovskite to the BO_3 lattice sketched in Fig. 1(a).

(ii) For the B sites, the relevant electronic orbital is non-degenerate and spatially well spread out, so that the onsite Hubbard repulsion can be safely ignored. This is a good approximation for BaBiO_3 , where this is the Bi:6s orbital. From

now we will call this the “ s ” orbital, and denote by $s_{i,\sigma}^\dagger$ the creation operator for a hole with spin σ in this orbital of the atom B in the unit cell i .

(iii) At each O site, we only keep in the model the $2p_\gamma$ orbital with ligand character, i.e., $\gamma = x, y, z$ for the O located on bonds parallel to x, y, z , respectively. We will refer to this as the x, y , or z orbital and use either the generic $\gamma_{i,\sigma}^\dagger$ operator when referring to any of the three O in the unit cell i or the specific $x_{i,\sigma}^\dagger, y_{i,\sigma}^\dagger, z_{i,\sigma}^\dagger$ for the creation operator associated with adding a hole to the O located on the x, y, z bond of unit cell i , see Fig. 1(b).

(iv) We ignore all phonon modes that are primarily located on A and B sites and instead keep only the optical phonon describing longitudinal (parallel to its ligand bond) oscillations of each O. The first part is reasonable as the A and B atoms are much heavier than O, so we expect their motion to mostly contribute to very low-energy phonon modes which do not couple strongly to the hole’s motion (see below). The second part is justified because to first order, one can think of each O as oscillating longitudinally between its two immobile B neighbors, with a characteristic frequency Ω that is the same at all O sites. For a crystal, this is equivalent with an Einstein phonon mode of frequency Ω on the O sites. In the following, we will denote the phonon creation operator for the $\gamma = \{x, y, z\}$ O site in unit cell i as $b_{i,\gamma}^\dagger$.

In this work, we focus on the effect of this phonon mode on the hybridization between neighbor O and B sites, as well as neighbor O sites. The resulting electron-phonon coupling is known as a Peierls coupling [28,31,32] and should be contrasted to the Rice-Sneddon model that focuses on the modulation of the onsite energy of a hole located in the s orbital, due to oscillatory motion of adjacent O. As discussed in the Introduction, the latter has been argued to be well modelled by an effective Holstein coupling on a simplified cubic lattice with only B sites included. Our results discussed below show that this equivalence with a Holstein model does not hold for the Peierls coupling in a considerable region of the parameter space.

To summarize, the Peierls model that we study is:

$$\hat{H} = \hat{H}_0 + \hat{V}, \quad (1)$$

where

$$\hat{H}_0 = \Omega \sum_{i,\gamma} b_{i\gamma}^\dagger b_{i\gamma} - \Delta \sum_{i,\gamma} \gamma_i^\dagger \gamma_i + T_{sp} + T_{pp} \quad (2)$$

describes the Einstein phonon modes (we set $\hbar = 1$), the charge-transfer energy Δ between p and s atomic orbitals, and the nearest neighbor (nn) s - p and p - p hopping, respectively, while

$$\hat{V} = H^{sp} + H^{pp} \quad (3)$$

is the Peierls electron-phonon coupling [28,31,32] describing the modulation of the s - p and p - p hoppings due to the O vibrations. Specifically:

$$T_{sp} = t \sum_{i,\gamma} s_i^\dagger (\gamma_i - \gamma_{i-\gamma}) + \text{H.c.}$$

$$T_{pp} = -t_p \sum_{i,\gamma} \gamma_i^\dagger (\gamma'_i - \gamma'_{i-\gamma'} - \gamma'_{i+\gamma} + \gamma'_{i+\gamma-\gamma'}) + \text{H.c.}$$

$$H^{sp} = -\alpha t \sum_{i,\gamma} [\gamma_i^\dagger (s_i + s_{i+\gamma})(b_{i\gamma}^\dagger + b_{i\gamma}) + \text{H.c.}]$$

$$H^{pp} = \beta t_p \sum_{i,\gamma} [\gamma_i^\dagger (\gamma'_i - \gamma'_{i-\gamma'} + \gamma'_{i+\gamma} - \gamma'_{i+\gamma-\gamma'})$$

$$+ \gamma''_i - \gamma''_{i-\gamma''} + \gamma''_{i+\gamma} - \gamma''_{i+\gamma-\gamma''})(b_{i\gamma}^\dagger + b_{i\gamma}) + \text{H.c.}],$$

where we use the short-hand notation:

$$\gamma' = \begin{cases} y, & \text{if } \gamma = x \\ z, & \text{if } \gamma = y; \\ x, & \text{if } \gamma = z \end{cases} \quad \gamma'' = \begin{cases} z, & \text{if } \gamma = x \\ x, & \text{if } \gamma = y \\ y, & \text{if } \gamma = z \end{cases}$$

in the above sums. We note that here and in the following we ignore the spin degree of freedom σ of the hole, which is irrelevant in the one-hole limit we study below.

Apart from Ω , the parameters are the charge-transfer energy Δ and the hopping integrals t and t_p for s - p and p - p hopping, respectively, when the O are at their equilibrium positions. The latter are negative numbers $t, t_p < 0$ for holes, with the additional signs due to the orbitals' overlaps explicitly written in the Hamiltonians above. Similarly, α and β characterize the electron-phonon couplings coming from the modulation of the s - p and p - p hoppings when the O are displaced out of their equilibrium positions. For holes, $\alpha, \beta > 0$ and according to Harrison's rule, $\beta = \alpha/2$ [35].

Finally, we note that the single electron case can be treated similarly, by appropriately changing the signs of the hoppings. In fact, it can be shown that the Hamiltonian with $t_p = 0$ is particle-hole symmetric, and thus the results are identical. A finite t_p breaks this symmetry so there will be quantitative, but not qualitative, differences between the single-hole and single-electron results. These will not affect our main conclusions.

The BO₆ cluster model

Density functional theory (DFT) studies of BaBiO₃ revealed that the most important hybridization is between the s orbital and the linear combination of neighbor O p orbitals with A_{1g} symmetry [29]. This stabilizes "molecular"-like orbitals with $s + p_{A_{1g}}$ character and suggests a possible mapping onto a simple cubic lattice by retaining only the lowest such state for each BO₆ cluster.

To test this hypothesis, we also investigate a single BO₆ cluster and the effects of Peierls coupling [28,31,32] on its spectrum. The Hamiltonian is that of Eq. (1) when limited to a single B site and its 6 O neighbors. For convenience, for the cluster case we choose a different convention for the signs of the $2p$ orbitals' lobes, as shown in Fig. 2.

The corresponding cluster model is:

$$\mathcal{H} = \Omega \sum_{i=1}^6 b_i^\dagger b_i + \Delta s^\dagger s - \sum_{i=1}^6 t (s^\dagger p_i + p_i^\dagger s)$$

$$- \sum_{i=1}^6 \alpha t (s^\dagger p_i + p_i^\dagger s)(b_i^\dagger + b_i)$$

$$- t_p \sum_{i=1,3,5} [(p_i^\dagger + p_{i+1}^\dagger)(p_{i+2} + p_{i+3}) + \text{H.c.}]$$

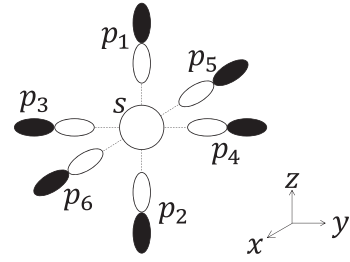


FIG. 2. BO₆ cluster with the central s orbital surrounded by six p ligand orbitals. Note that for convenience, here we use a different convention for the signs of the p_1, p_4 , and p_6 orbitals than used in the lattice case depicted in Fig. 1.

$$- \beta t_p [[p_6^\dagger (b_6^\dagger + b_6) + p_5^\dagger (b_5^\dagger + b_5)](p_4 + p_3)$$

$$+ (p_5^\dagger + p_6^\dagger)[p_3 (b_3^\dagger + b_3) + p_4 (b_4^\dagger + b_4)] + \dots], \quad (4)$$

where i labels are cyclic with period 6. We only list here a few of the terms in H^{pp} (the last two lines); the full expression is given in Appendix A. All the parameters have the same meaning as in Hamiltonian (1).

The cluster Hamiltonian can be written more simply in terms of hole and boson operators consistent with its symmetry. We define the new hole operators:

$$P_1 = \frac{1}{\sqrt{6}}(p_1 + p_2 + \dots + p_6)$$

$$P_2 = \frac{1}{\sqrt{12}}(2p_1 + 2p_2 - p_3 - p_4 - p_5 - p_6)$$

$$P_3 = \frac{1}{\sqrt{4}}(p_5 + p_6 - p_3 - p_4)$$

$$P_4 = \frac{1}{\sqrt{2}}(p_6 - p_5)$$

$$P_5 = \frac{1}{\sqrt{2}}(p_4 - p_3)$$

$$P_6 = \frac{1}{\sqrt{2}}(p_1 - p_2)$$

and similarly for the boson operators: $B_1 = \sum_{i=1}^6 b_i$, etc. P_1^\dagger creates a hole in the linear combination of O $2p$ orbitals with A_{1g} (s -like) symmetry, P_2^\dagger and P_3^\dagger correspond to the E_g terms with $d_{3z^2-r^2}$ and $d_{x^2-y^2}$ symmetry, respectively, and P_4^\dagger, P_5^\dagger and P_6^\dagger correspond to the T_{1u} terms with p_x, p_y , and p_z symmetry, respectively. We define the new bosonic operators B_i similarly.

In the new basis, the cluster Hamiltonian becomes:

$$\mathcal{H} = \Omega \sum_{i=1}^6 B_i^\dagger B_i + \Delta s^\dagger s - T (s^\dagger P_1 + P_1^\dagger s)$$

$$- \alpha t \sum_{i=1}^6 (s^\dagger P_i + P_i^\dagger s)(B_i^\dagger + B_i)$$

$$- t_p (4P_1^\dagger P_1 - 2P_2^\dagger P_2 - 2P_3^\dagger P_3)$$

$$- \beta t_p \left(\sqrt{\frac{8}{3}} (B_1^\dagger + B_1)(2P_1^\dagger P_1 - P_2^\dagger P_2 - P_3^\dagger P_3) + \dots \right), \quad (5)$$

where the dots in the last line refer to terms involving phonon operators $B_i + B_i^\dagger$ with $i \neq 1$, i.e., the other E_g and T_{1u} symmetries are included. The complete Hamiltonian can be found in Appendix A. Note that because of the pp hopping, the effective charge transfer energy between the s and the P_1 molecular orbital is $\Delta_1 = \Delta + 4t_p$, whereas for the E_g molecular orbitals, the effective charge transfer energy is $\Delta_2 = \Delta_3 = \Delta - 2t_p$.

The third term shows that indeed the s orbital only hybridizes with the P_1 molecular orbital with the same A_{1g} symmetry, and the effective hopping is $T = \sqrt{6}t$. However, because the presence of deformations breaks this symmetry, the Peierls α electron-phonon coupling [28,31,32] allows hopping between the s and any of the P_i orbitals, if bosons with the same symmetry i are either already present or are being created during the process—see terms on the second line. Terms generated by the modulation of the p - p hopping can be understood similarly.

III. METHODS

We studied the models described above by a variety of means which we briefly review here, with full details relegated to various Appendixes.

A. Perturbation theory for the lattice case in the adiabatic limit

In the adiabatic limit where Ω is the largest energy scale, we can use perturbation theory to project out the high-energy states with one or more phonons to obtain an effective Hamiltonian describing the motion of the polaron. The resulting analytical dispersion is useful because it allows us to gain intuition about the behavior of the polaron in this limit, as discussed below.

We partition the Hamiltonian into $\hat{H} = \hat{h}_0 + \hat{h}_1$, where $\hat{h}_0 \equiv \Omega \sum_{i,\gamma} b_{i\gamma}^\dagger b_{i\gamma}$ is the large part, and \hat{h}_1 includes all the other terms and is treated as the perturbation. Using standard second order perturbation theory (PT) [36], we obtain the low-energy effective Hamiltonian to be:

$$\hat{h} = \hat{h}_0 + \hat{P}_0 \hat{h}_1 \hat{P}_0 + \hat{P}_0 \hat{h}_1 \frac{1 - \hat{P}_0}{E_0 - \hat{h}_0} \hat{h}_1 \hat{P}_0 + \mathcal{O}\left(\frac{1}{\Omega^2}\right),$$

where \hat{P}_0 is the projection operator onto the highly-degenerate, one-hole ground state manifold of \hat{h}_0 , i.e., zero-phonon states with energy $E_0 = 0$.

After carrying out these calculations, we find that $\hat{h} = -\Delta \sum_{i\gamma} \gamma_i^\dagger \gamma_i + T_{sp} + T_{pp} + \delta\hat{h} + \mathcal{O}\left(\frac{1}{\Omega^2}\right)$ where:

$$\delta\hat{h} = -\frac{\alpha^2 t^2}{\Omega} \sum_{j\gamma} (\tilde{s}_{j,\gamma}^\dagger + \tilde{s}_{j-\gamma,\gamma}^\dagger) s_j - \frac{2\alpha^2 t^2 + 8\beta^2 t_p^2}{\Omega} \sum_{j\gamma} \gamma_j^\dagger \gamma_j + \frac{\alpha\beta t t_p}{\Omega} \sum_{j\gamma} (\tilde{\gamma}_{j,\gamma'}^\dagger + \tilde{\gamma}_{j,\gamma''}^\dagger + \tilde{\gamma}_{j-\gamma,\gamma'}^\dagger + \tilde{\gamma}_{j-\gamma,\gamma''}^\dagger) s_j$$

$$\begin{aligned} & - \frac{\alpha\beta t t_p}{\Omega} \sum_{j\gamma} (-\tilde{s}_{j,\gamma''}^\dagger + \tilde{s}_{j+\gamma,\gamma''}^\dagger - \tilde{s}_{j-\gamma'',\gamma''}^\dagger + \tilde{s}_{j+\gamma-\gamma'',\gamma''}^\dagger \\ & - \tilde{s}_{j,\gamma'}^\dagger + \tilde{s}_{j+\gamma,\gamma'}^\dagger - \tilde{s}_{j-\gamma',\gamma'}^\dagger + \tilde{s}_{j+\gamma-\gamma',\gamma'}^\dagger) \gamma_j \\ & - \frac{\beta^2 t_p^2}{\Omega} \sum_{j\gamma} (\tilde{\gamma}_{j,\gamma}''\dagger + \tilde{\gamma}_{j,\gamma}'\dagger - \tilde{\gamma}_{j+\gamma,\gamma}''\dagger - \tilde{\gamma}_{j+\gamma,\gamma}'\dagger + \tilde{\gamma}_{j-\gamma,\gamma}''\dagger \\ & + \tilde{\gamma}_{j-\gamma,\gamma}'\dagger - \tilde{\gamma}_{j+\gamma-\gamma'',\gamma}''\dagger - \tilde{\gamma}_{j+\gamma-\gamma'',\gamma}'\dagger + \tilde{\gamma}_{j,\gamma}''\dagger \\ & + \tilde{\gamma}_{j,\gamma}'\dagger - \tilde{\gamma}_{j+\gamma,\gamma''}\dagger - \tilde{\gamma}_{j+\gamma,\gamma}'\dagger + \tilde{\gamma}_{j-\gamma,\gamma}''\dagger \\ & + \tilde{\gamma}_{j-\gamma',\gamma}''\dagger - \tilde{\gamma}_{j+\gamma-\gamma',\gamma''}\dagger - \tilde{\gamma}_{j+\gamma-\gamma',\gamma}'\dagger) \gamma_j \end{aligned} \quad (6)$$

and we used the short-hand notation:

$$\begin{aligned} \tilde{s}_{j,\gamma}^\dagger & \equiv s_j^\dagger + s_{j+\gamma}^\dagger \\ \tilde{\gamma}_{j,\gamma'}^\dagger & \equiv \gamma_j^\dagger - \gamma_{j-\gamma'}^\dagger + \gamma_{j+\gamma}^\dagger - \gamma_{j+\gamma-\gamma'}^\dagger. \end{aligned}$$

The expression of $\delta\hat{h}$ may seem complicated, but it consists of simple terms whose appearance is conceptually straightforward to understand. They can be divided into onsite energies like $-6\alpha^2 t^2 / \Omega \sum_j s_j^\dagger s_j$ (part of the first term on the first line), which reflect the polaron formation energy as a hole located at an s site hops to a neighbor O and back while creating and then reabsorbing a phonon at that O site. The onsite energy at the O sites is also renormalized (last term on the first line) but by a different amount, so together these two terms imply a change of the effective Δ .

All other terms describe longer-range hopping *dynamically generated* through phonon emission+absorption. For example, the first term on the first line contains terms proportional to $s_{j'}^\dagger s_j$, where j' and j are nn neighbor s orbitals. These terms are generated when a hole hops from site j to the O located in between j and j' while creating a phonon at that O and then hops again while absorbing the phonon and lands at site j' . Similar processes generate additional s - p and p - p hoppings, which supplement and renormalize the bare hopping $T_{sp} + T_{pp}$ and will therefore modify the polaron dispersion.

To find the polaron dispersion, we Fourier transform \hat{h} . For any \mathbf{k} point in the cubic Brillouin zone, we get a 4×4 matrix that can be diagonalized numerically. In the following, we focus on the lowest-energy band in order to trace its evolution, in particular how the momentum of the ground state evolves in the parameter space.

B. Perturbation theory for the lattice case for weak electron-phonon coupling

Another case that can be treated with standard PT is when the electron-phonon coupling $\alpha \rightarrow 0$. For simplicity, we set $\beta = 0$ and treat only the equivalent 1D case [37]—this suffices for our needs. The more general 3D case with $\beta \neq 0$ can be treated similarly.

Using Rayleigh-Schrödinger perturbation to second order, the polaron energy is:

$$\begin{aligned} E_P(k) = E_0(k) + \frac{(\alpha t)^2}{8\pi} \int_{-\pi}^{\pi} dq \left[- (1 + e^{-i(k-q)})(1 + e^{iq}) \left(\frac{1}{E_0(k) - \Omega - E_0(k-q)} - \frac{1}{E_0(k) - \Omega + E_0(k-q)} \right) \right. \\ \left. + (1 + e^{-i(k-q)})(1 + e^{i(k-q)}) \left(\frac{1}{E_0(k) - \Omega - E_0(k-q)} + \frac{1}{E_0(k) - \Omega + E_0(k-q)} \right) \right] \end{aligned}$$

$$\begin{aligned}
& + (1 + e^{ik})(1 + e^{-ik}) \left(\frac{1}{E_0(k) - \Omega - E_0(k+q)} + \frac{1}{E_0(k) - \Omega + E_0(k+q)} \right) \\
& - (1 + e^{-ik})(1 + e^{i(k+q)}) \left(\frac{1}{E_0(k) - \Omega - E_0(k+q)} - \frac{1}{E_0(k) - \Omega + E_0(k+q)} \right) \Big] \quad (7)
\end{aligned}$$

where $E_0(k) = -|2t \sin(k/2)|$ is the free-hole dispersion and $a = 1$. This result is only valid for phonon energy $\Omega > 2|t|$, because otherwise the denominators vanish for large enough k (Brillouin-Wigner PT must be used in this case). For $\alpha = 0$, the GS is at $k = \pi$ and has energy $E_0(\pi) = -2|t|$, while $E_0(0) = 0$. Note the additional phase factors inside the integrand. These appear because the Peierls electron-phonon vertex, when Fourier transformed, depends explicitly on both the hole momentum k and the phonon momentum q . This (k, q) dependence is a direct consequence of the nondiagonal nature of the Peierls coupling and is very unlike the Holstein model, where this vertex is a constant.

C. Momentum average (MA) approximation for the lattice case

The two methods introduced above are only accurate in the asymptotic limits of very large phonon frequencies

and/or very weak electron-phonon coupling. To gain an understanding of what happens in other regions of the parameter space, we use MA, which is a variational method [38–42] for calculating the one-hole Green's functions $G^{\beta\alpha}(\mathbf{k}, \omega) \equiv \langle 0 | \beta_{\mathbf{k}} \hat{G}(\omega) \alpha_{\mathbf{k}}^\dagger | 0 \rangle$, where $\alpha, \beta \in \{s, x, y, z\}$ are any pair of orbitals, $\hat{G}(\omega) = [\omega + i\eta - \hat{H}]^{-1}$ is the resolvent for the Hamiltonian of Eq. (1), and $|0\rangle$ is the vacuum for holes and phonons.

Here we present a brief overview of MA, with technical details relegated to Appendix B. To find $G^{\beta\alpha}(\mathbf{k}, \omega)$, we use Dyson's identity: $\hat{G}(\omega) = \hat{G}_0(\omega) + \hat{G}(\omega) \hat{V} \hat{G}_0(\omega)$, where \hat{H}_0 is the Hamiltonian of Eq. (2), $\hat{V} = \hat{H} - \hat{H}_0$, and $\hat{G}_0(\omega) = [\omega + i\eta - \hat{H}_0]^{-1}$ is the resolvent for \hat{H}_0 , whose corresponding propagators $G_0^{\beta\alpha}(\mathbf{k}, \omega) = \langle 0 | \beta_{\mathbf{k}} \hat{G}_0(\omega) \alpha_{\mathbf{k}}^\dagger | 0 \rangle$ can be calculated by Chebyshev Polynomials expansion, as explained in Appendix C. Using Dyson's identity leads to the exact equation:

$$\begin{aligned}
G^{\beta\alpha}(\mathbf{k}, \omega) &= G_0^{\beta\alpha}(\mathbf{k}, \omega) - \alpha t \sum_{\gamma} (1 + e^{i\mathbf{k}\cdot\mathbf{r}_\gamma}) \tilde{f}_{\gamma,\gamma}^{(1)} G_0^{s\alpha}(\mathbf{k}, \omega) \\
&\quad - \sum_{\gamma} [\alpha t \tilde{f}_{s,\gamma}^{(1)} - \beta t_p (\tilde{f}_{\gamma',\gamma}^{(1)} + \tilde{f}_{\gamma'',\gamma}^{(1)} + \xi_{\gamma''\gamma}(\mathbf{k}) \tilde{f}_{\gamma'',\gamma''}^{(1)} + \xi_{\gamma'\gamma}(\mathbf{k}) \tilde{f}_{\gamma',\gamma'}^{(1)})] G_0^{\gamma\alpha}(\mathbf{k}, \omega), \quad (8)
\end{aligned}$$

where we defined the generalized propagators

$$f_{\gamma,\delta,\ell}^{(n)}(\mathbf{k}, \omega) \equiv \sum_j \frac{e^{i\mathbf{k}R_j}}{N} \langle 0 | \beta_{\mathbf{k}} \hat{G}(\omega) \gamma_{j+\ell}^\dagger (b_{j\delta}^\dagger)^n | 0 \rangle \quad (9)$$

and we use the short-hand notations:

$$\begin{aligned}
\xi_{\gamma_1,\gamma_2}(\mathbf{k}) &\equiv 1 - e^{-i\mathbf{k}\cdot\mathbf{r}_{\gamma_2}} + e^{i\mathbf{k}\cdot\mathbf{r}_{\gamma_1}} - e^{i(\mathbf{k}\cdot\mathbf{r}_{\gamma_1} - \mathbf{k}\cdot\mathbf{r}_{\gamma_2})} \\
\tilde{f}_{s,\gamma}^{(n)} &\equiv f_{s,\gamma,0}^{(n)} + f_{s,\gamma,\gamma}^{(n)} \\
\tilde{f}_{\gamma,\gamma}^{(n)} &\equiv f_{\gamma,\gamma,0}^{(n)} \\
\tilde{f}_{\gamma_1,\gamma_2}^{(n)} &\equiv f_{\gamma_1,\gamma_2,0}^{(n)} - f_{\gamma_1,\gamma_2,-\gamma_1}^{(n)} + f_{\gamma_1,\gamma_2,\gamma_2}^{(n)} - f_{\gamma_1,\gamma_2,\gamma_2-\gamma_1}^{(n)}
\end{aligned}$$

in which the dependence on (\mathbf{k}, ω) of the various f propagators is not written explicitly for brevity.

To find equations of motion for the various $f^{(1)}$ propagators appearing in Eq. (8), we apply again Dyson's identity. The electron-phonon coupling terms either remove the phonon, linking the various $f^{(1)}$ back to various $G^{\beta\alpha}(\mathbf{k}, \omega)$, or add a phonon and thus also link to new propagators with two phonons present in the initial (ket) state. If the two phonons are on the same O site, the corresponding propagator is one of the $f^{(2)}$ defined in Eq. (9) and we keep it, but we ignore the propagators with phonons located on different sites. The same procedure is employed to generate equations of motion for all $f^{(n)}$ for any $n \geq 2$, linking them to various $f^{(n-1)}$ and $f^{(n+1)}$.

The resulting equations, listed in Appendix B where we also discuss their solution, implement the variational guess [40–42] that the largest weight to the polaron cloud comes from configurations where all phonons are at the same O site. That this should be a reasonable choice can be seen as follows: (i) If the hole is at an O site that is already displaced, i.e., it has phonons, the Peierls electron-phonon coupling α will hop it to one of its neighbor B sites and create an additional phonon at the original O site—this process is included in our variational calculation. The Peierls electron-phonon coupling β will hop the hole to an adjacent O site, creating a new phonon either at the original O site (a process we include) or at the new O site (a process we ignore, because now there would be phonons on two different sites). Similarly, if (ii) the hole is at a B site neighbor to an O with several phonons, then a Peierls α process can take the hole back to the displaced O site, adding to the number of phonons there (we keep this) or to a different O site (we dismiss this as it would add a phonon at the new site). The reason is that each phonon costs an energy Ω but the hole cannot take advantage of (interact simultaneously with) phonons on multiple sites, so the most advantageous low-energy approach is to keep the phonon cloud spatially small.

We have tested this intuition for the 1D version of this model in Ref. [37], where we compared the MA results against those of exact diagonalization (ED) with excellent success. ED is prohibitively expensive in higher dimensions, but

we know from extensive studies of MA for other models that its accuracy improves with increasing dimensionality [38–40]. Mathematically, this is a consequence of the fact that all else being equal, propagators in higher dimensions decrease faster with increasing distance. As mentioned above, the variational constraint implemented here is that we only keep configurations with phonons on one site. To create a spatially more extended cloud, the electron has to travel between sites hosting phonons. Such processes will have a very small amplitude of probability if the propagator to move between different sites is very small, which is indeed the case at energies lying below the free particle bands.

Additionally, MA accuracy can be gauged by increasing the variational space. The simplest new configurations are those allowing an extra phonon on a different site than the one that already has a cloud. For the 1D and 2D versions of this model we found that including these additional states has very small influence on the results, for instance changing eigenenergies by very few percent, so long as the phonon frequency is not very small compared to the free electron bandwidth [37,43]. (It is well documented that MA becomes less accurate in the adiabatic limit [39,40], which is why here we only show MA results for sufficiently large Ω where we trust our results to be accurate within a few percent). We have not implemented an expanded variational MA calculation for the 3D case discussed here because it becomes mathematically quite cumbersome and small quantitative changes would not affect the qualitative conclusions we draw below.

D. Variational approximation for the cluster Hamiltonian

The spectrum of the cluster Hamiltonian of Eq. (5) can be found by exact diagonalization, but for our purposes it suffices to use a variational approximation that sets an upper bound to the ground-state energy. The best trial wave function we found is:

$$|\psi_v\rangle = \frac{s^\dagger + \sum_{i=1}^6 \chi_i P_i^\dagger}{\sqrt{1 + \sum_{i=1}^6 \chi_i^2}} \prod_{i=1}^6 e^{-\frac{1}{2}\eta_i^2 + \eta_i B_i^\dagger} |0\rangle, \quad (10)$$

where χ_i and η_i are the variational parameters. After some algebra, we find:

$$\langle \psi_v | \mathcal{H} | \psi_v \rangle = \frac{\Delta - 2t\chi_1}{1 + \sum_i \chi_i^2} + \Omega \sum_i \eta_i^2 - \frac{4\alpha t \sum_i \chi_i \eta_i}{1 + \sum_i \chi_i^2} + \dots,$$

where the dots are terms from p - p hopping, which we do not write here explicitly but we did include when generating the results shown below. This is minimized to find an upper bound for the cluster GS energy, which we refer to as the “variational” cluster energy.

E. A_{1g} approximation for the cluster Hamiltonian

Given that the s orbital only hybridizes with the P_1 orbital with a large $T = \sqrt{6}t$, one may expect that the terms with A_{1g} symmetry contribute most to the ground state. We could then remove from the cluster Hamiltonian the terms with boson operators of other symmetries and still expect a good low-energy description.

The resulting simplified cluster Hamiltonian is:

$$\begin{aligned} \mathcal{H}_{A_{1g}} &= \Delta s^\dagger s + \Omega B_1^\dagger B_1 - T(s^\dagger P_1 + P_1^\dagger s) \\ &\quad - \alpha t(s^\dagger P_1 + P_1^\dagger s)(B_1^\dagger + B_1) \\ &\quad - 4t_p P_1^\dagger P_1 - 4\sqrt{\frac{2}{3}}\beta t_p P_1^\dagger P_1 (B_1^\dagger + B_1). \end{aligned} \quad (11)$$

Its ground state energy can be found using continued fractions [44], see Appendix D. We refer to it as the “ A_{1g} ” cluster energy.

F. Holstein approximation for the cluster Hamiltonian

We rewrite the electronic part of $\mathcal{H}_{A_{1g}}$ in terms of the (for holes) bonding $d_1^\dagger = (s^\dagger - P_1^\dagger)/\sqrt{2}$ and antibonding $d_2^\dagger = (s^\dagger + P_1^\dagger)/\sqrt{2}$ operators. For $T \gg \Delta$, the bonding orbital is located about $2T$ below the antibonding one, and we expect to get a good low-energy approximation by ignoring all terms involving d_2 operators.

The resulting simplified cluster Hamiltonian is:

$$\mathcal{H}_H = \epsilon d_1^\dagger d_1 + \Omega B_1^\dagger B_1 + g_H d_1^\dagger d_1 (B_1^\dagger + B_1).$$

This defines a one-site Holstein model with effective parameters $\epsilon = \frac{\Delta}{2} - T - 2t_p$ and $g_H = \alpha t - 2\sqrt{\frac{2}{3}}\beta t_p$. It can be solved exactly and has a one-hole ground-state energy $E_H = \epsilon - g_H^2/\Omega$. In the following, we refer to this as the “Holstein” cluster energy.

By comparing the variational, A_{1g} , and Holstein cluster energies, we can infer the validity of these various approximations in different regions of the parameter space, to see when/if a Holstein model provides a good low-energy description of the cluster. Together with the results for the lattice case, this will allow us to understand the equivalence (or lack thereof) between the Peierls and the Holstein models on the perovskite lattice.

IV. RESULTS

In this section, the values chosen for the various parameters are for illustration purposes, so that a broad region of the parameter space can be sampled. Results specific to the values we believe to be appropriate for BaBiO₃ are presented and discussed in the last section.

A. Results for the cluster

Figure 3 compares the cluster ground-state energies E_{gs} obtained with the variational (symbols), A_{1g} (full line) and Holstein (dashed line) approximations. In all cases, we use $|t| = 1$ as the unit of energy. Panels (a) and (e) show the evolution of E_{gs} with the Peierls coupling α (with $\beta = \alpha/2$ used throughout), when $t_p = 0$ and $\Delta = 0$. The phonon frequency is $\Omega = 0.1$ in panel (a) and $\Omega = 2$ in panel (e). The three approximations are in very good agreement. The same is true for panels (b) and (f), where we track the dependence of E_{gs} on Ω . Here, we continue to keep $t_p = \Delta = 0$, and we set the Peierls coupling $\alpha = 0.2$ in panel (b) and $\alpha = 1.2$ in panel (f). We conclude that for vanishing Δ and p - p hopping, a Holstein description is very satisfactory for the cluster for all phonon frequencies and electron-phonon couplings.

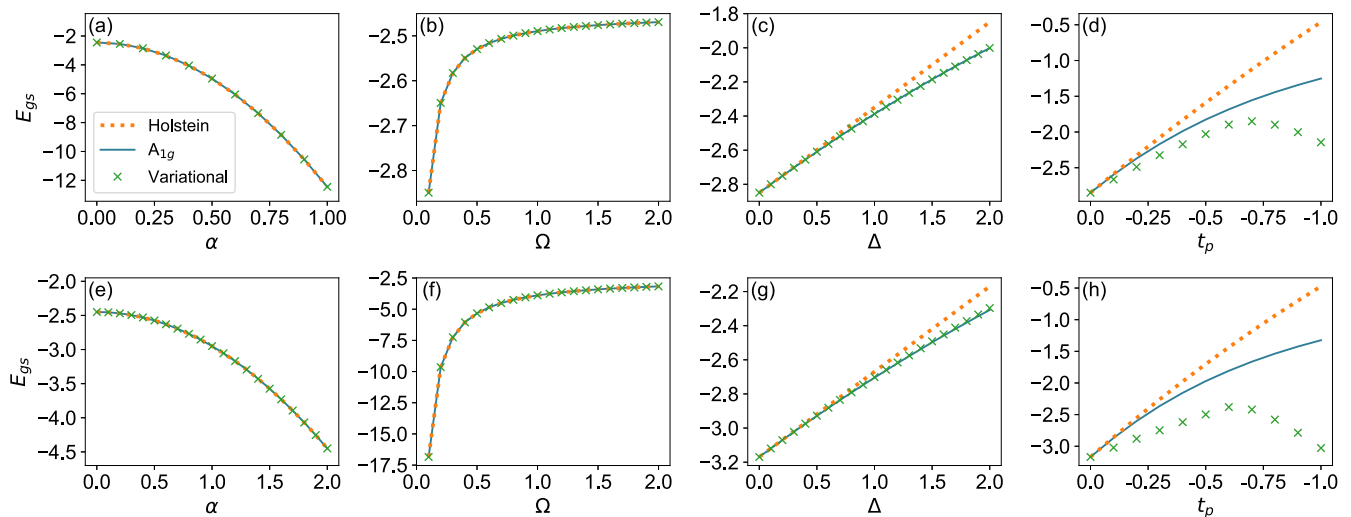


FIG. 3. Comparison between the cluster ground state energies obtained with the variational (symbols), A_{1g} (full line) and Holstein (dashed line) approximations, respectively, as a function of various parameters. If not otherwise specified, parameters used in (a)–(d) are $t = -1$, $t_p = 0$, $\Delta = 0$, $\Omega = 0.1$, and $\alpha = 0.2$ and in (e)–(h) $t = -1$, $t_p = 0$, $\Delta = 0$, $\Omega = 2$, and $\alpha = 1.2$. In all cases, $\beta = \frac{\alpha}{2}$.

This is no longer the case, however, when either $\Delta \neq 0$ and/or $t_p \neq 0$. In panels (c) and (g) we track the dependence of E_{gs} on Δ , when $t_p = 0$ and $\Omega = 0.1$, $\alpha = 0.2$ in panel (c), versus $\Omega = 2$, $\alpha = 1.2$ in panel (g). Both cases show good agreement between the variational and the A_{1g} results, suggesting that the cluster distortion remains s -like. However, projecting out the antibonding orbital becomes increasingly inaccurate with increasing Δ . This is because a large Δ favors a different mix between the s and P_1 orbitals than the 50/50 mix favored by the hybridization T and by the electron-phonon coupling, see Eq. (11). As a result, there is no unique choice for a single “cluster” low-energy electronic orbital onto which to project, thus a Holstein-like description becomes increasingly inaccurate.

The problem is further exacerbated if we add a finite t_p hopping. This term is known to be important because it is primarily responsible for setting the bandwidth of the O band, which is generally considerable in perovskites. Physically, this is a consequence of the rather short distance between adjacent O, which means that t_p is not negligible compared to t . As already noted, it also decreases the effective charge transfer energy between the s and P_1 orbitals. The dependence of E_{gs} on $|t_p|$ is shown in panels (d) and (h). In both cases $\Delta = 0$, and the values of the other parameters are as in (c) and (g), respectively. For any finite t_p , the A_{1g} approximation fails rather fast, and the Holstein one is even worse. The reason is that the β Peierls coupling connects the s -like O distortion described by B_1, B_1^\dagger not just to the P_1 orbital with A_{1g} symmetry but also to the E_g orbitals P_2, P_3 , see Eq. (5). In term, when the electron occupies one of these other orbitals, it favors the appearance of distortions with the same symmetry, see the α term in Eq. (5). The end result is that the other distortion modes are also activated, so now even the projection onto the A_{1g} symmetry is inaccurate, making the further steps to a Holstein mapping impossible.

Indeed, we find that the downturn of the variational energy at larger t_p occurs because the E_g symmetry starts to dominate over the A_{1g} one, as shown by their weights in the variational

calculation (not shown here). This is reminiscent of the phase transition [30] in BaBiO_3 between the A_{1g} dominated bond-disproportionated state and the E_g metallic state, driven by the change of effective charge transfer energy $\Delta_1 = \Delta + 4t_p$.

It is important to emphasize that the activation of the cluster bosonic modes with other E_g symmetries does not necessarily imply a nonsymmetric distortion of the O cage (i.e., one breaking the cubic symmetry), so far as the average distortion is concerned. For example, activation of the B_3 ($x^2 - y^2$) distortion will either bring the O on the x bonds closer and push the y bonds O further out or vice versa. A wave function which has equal contributions from both positive and negative B_3 distortions will, in average, retain the cubic symmetry. To conclude, the cluster results already demonstrate that an effective Holstein description is likely to fail for realistic systems with finite charge-transfer energies $\Delta \neq 0$ and finite p - p -hopping $t_p \neq 0$.

B. Results for the lattice

As just shown, the cluster results indicate that the Holstein mapping is not valid in parts of the parameter space. We expect this conclusion to be even stronger for the lattice case, given its lower symmetry group.

We begin in the antiadiabatic limit $\Omega \gg t$. As mentioned, this limit is not very physical: Most materials are rather in the adiabatic limit, although this may change for “flat-band” materials. However, here we can use PT predictions to verify and validate the MA results, and moreover, the effective PT Hamiltonian allows us to understand the results. As we then show further below, the qualitative behavior remains similar for all values of Ω , so gaining first intuition in this regime is valuable.

We first set $\Delta = 0$, $t_p = 0$ and study the evolution of the polaron dispersion with increasing $\alpha = 4.8, 5, 5.2$ (and $\beta = \alpha/2$) for $\Omega = 80$, $|t| = 1$. The results are shown in Fig. 4 (MA and PT results are identical in this limit). As customary, the high-symmetry points in the cubic Brillouin zone are

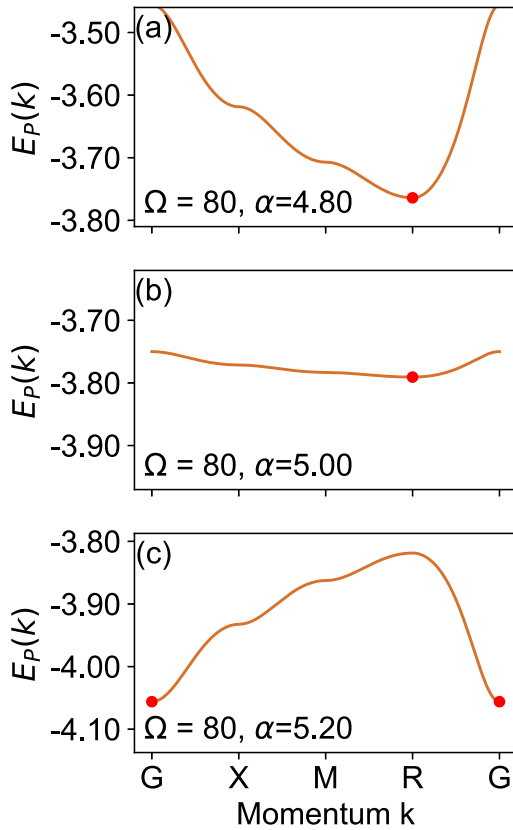


FIG. 4. Polaron dispersion in the antiadiabatic limit. These are perturbational results but in excellent agreement with the MA results. Parameters are $|t| = 1$, $t_p = \Delta = 0$, $\Omega = 80$ and (a) $\alpha = 4.8$, (b) $\alpha = 5$, and (c) $\alpha = 5.2$. Red dots indicate the ground state.

$G = (0, 0, 0)$, $M = (\pi, \pi, 0)$, $X = (\pi, 0, 0)$, and $R = (\pi, \pi, \pi)$ (we set $a = 1$).

For a Holstein model, the polaron dispersion has roughly the same shape as the free-hole band, but its bandwidth decreases monotonically with increasing electron-phonon coupling. In contrast, here we see that for $\alpha > 5$, the bandwidth starts to increase again. This is associated with a sharp switch of the momentum of the ground state from R to G , i.e., a change of the shape of the dispersion that is impossible for a Holstein model [34]. In Fig. 5(a) we show the location of this

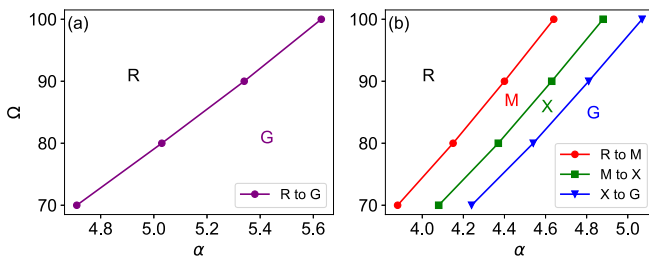


FIG. 5. (a) Ground state momentum \mathbf{k}_{gs} in the (Ω, α) parameter space, showing a sharp transition from $\mathbf{k}_{gs} = R$ to $\mathbf{k}_{gs} = G$. Here, $|t| = 1$, $t_p = 0$, $\Delta = 0$. (b) Same as in (a) but for $t_p = -0.2$. In this case, \mathbf{k}_{gs} moves from $R \rightarrow M \rightarrow X \rightarrow G$.

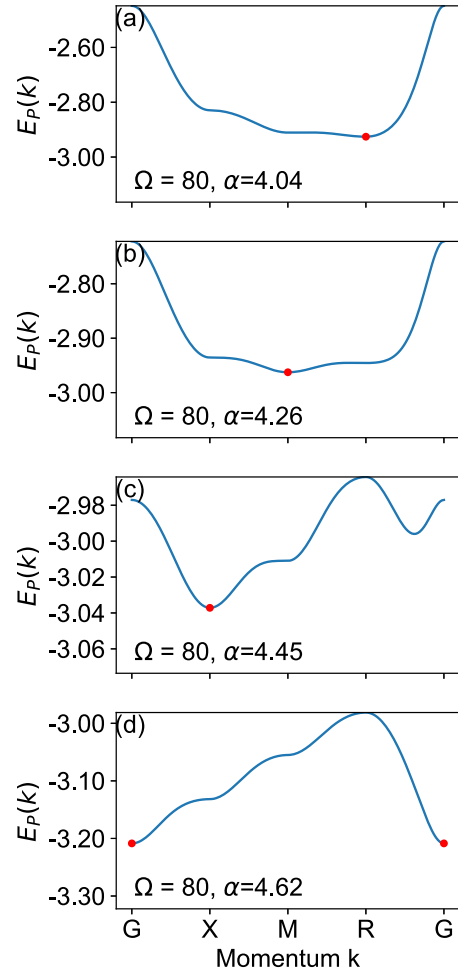


FIG. 6. Evolution of the polaron dispersion with α , when $t_p = -0.2$. Parameters not explicitly listed in the panels are as for Fig. 4.

sharp transition in the (α, Ω) plane, when $t_p = 0$, $\Delta = 0$ and $\Omega \gg 1$.

We now consider what happens when $\Delta \neq 0$, $t_p \neq 0$. We find that if $t_p = 0$, setting $\Delta \neq 0$ simply shifts the location of the transition in the parameter space (not shown). More spectacular is the case $t_p \neq 0$, where as α increases, we find not one but three closely spaced ground-state transitions from $R \rightarrow M \rightarrow X \rightarrow G$, see Fig. 5(b). The evolution of the polaron dispersion across these transitions is shown in Fig. 6.

Similar sharp transitions (sudden jumps) of the GS momentum between high-symmetry points have also been found for the 1D and 2D versions of this model, see Refs. [37,43,45]. They can be understood in several ways.

In the antiadiabatic limit, PT shows that the main effect of the Peierls electron-phonon coupling is to dynamically generate longer-range hopping terms and to renormalize the charge-transfer energy, see $\delta\hbar$ of Eq. (6) and following discussion. These longer-range hoppings favor a different \mathbf{k}_{gs} than that of the bare-hole dispersion, and thus the transition occurs when the electron-phonon coupling is strong enough that these new terms dominate the polaron dispersion. For $t_p \neq 0$, the number of such phonon-mediated longer-range hoppings increases further and the resulting, more complex polaron

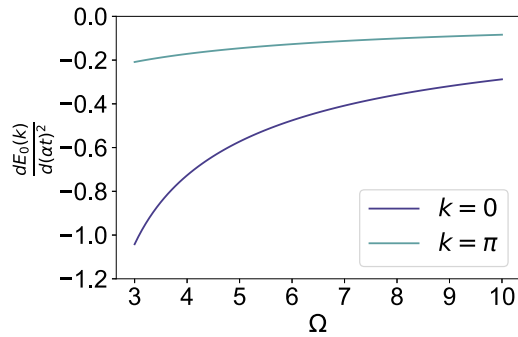


FIG. 7. Measure of the polaron energy $E_p(k)$ on the coupling α , in the limit $\alpha \rightarrow 0$. Note that for $k = 0$, the polaron energy decreases faster with α than for $k = \pi$. These are 1D results obtained with weak-coupling PT of Eq. (7). Parameters are $t = -1$, $t_p = 0$, $\Delta = 0$.

dispersion has more transitions. More discussion along these lines is available in Ref. [37].

This argument, however, is predicated on the system being in the antiadiabatic limit, and thus one might wonder if similar physics is seen at lower, more physical values of Ω . Before showing results proving that this is indeed the case, we provide a second argument explaining the origin of the k_{gs} jump(s). This is based on PT for weak electron-phonon coupling. For simplicity, we carry out this analysis for the 1D equivalent of our 3D model.

As shown in Eq. (7), the PT expression for $E_p(k)$ depends on k not just through the usual energy denominators but also because of the explicit (k, q) dependence of the Peierls electron-phonon vertex. The latter essentially means that holes with different momenta k couple with different strengths to the phonons, and this will affect how fast their energy is lowered with increasing α . Indeed, in Fig. 7 we plot $dE_p(k)/d(\alpha t)^2$ when $\alpha \rightarrow 0$, as a measure of this dependence of $E_p(k)$ on α . Both at $k = 0$ and at $k = \pi$ the values are negative, as expected, showing a lowering of the energy in the presence of electron-phonon coupling. However, the slopes are very different, with $E_p(0)$ moving faster towards lower energies than $E_p(\pi)$. This explains how it is possible that at a large enough α , the GS momentum will switch from the free-hole value $k_{gs} = \pi$ to $k_{gs} = 0$, instead. Also note that this difference is enhanced as one moves towards the adiabatic limit, suggesting that the existence of the transition(s) should be expected for any Ω , not just in the antiadiabatic limit. We confirm this below.

We now use MA to show that qualitatively similar behavior is seen at lower, more physical values of Ω where PT cannot be used. Indeed, we find that the sharp transitions persist, specifically again if $t_p = 0$ there is one from $R \rightarrow G$, see Fig. 8(a), and if $t_p \neq 0$ there are three from $R \rightarrow M \rightarrow X \rightarrow G$, see Fig. 8(b). In panel (b) we also show the slight shift of these transition lines if we set $\Delta = 1$. The shape and evolution of the spectra for various α is shown in Fig. 9 and are consistent with those found in the antiadiabatic limit. One challenge with using MA is that it is hard to accurately calculate the free-hole propagators $G_0^{\alpha\beta}(\mathbf{k}, \omega)$ for this complicated lattice, as they have fast oscillations in their ω dependence due to the finite cutoff in the Chebyshev polynomials expansion and the

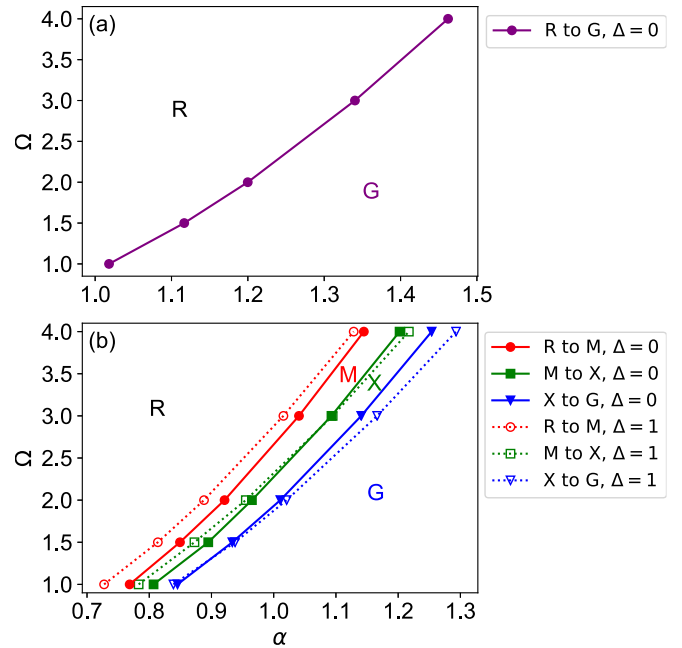


FIG. 8. Ground state momentum transitions in the (α, Ω) space, for smaller Ω . Panel (a) is for $t_p = \Delta = 0$; panel (b) is for $t_p = -0.2$, $\Delta = 0$ (solid lines) and $t_p = -0.2$, $\Delta = 1$ (dotted lines). Error bars are smaller than the size of the symbols. In the MA calculations used to generate this data, 101^3 unit cells are used for the 3D lattice and 500 terms are summed in the Chebyshev expansions for the free-hole propagators $G_0^{\alpha\beta}(\mathbf{k}, \omega)$. Other parameters are $t = -1$ and $\eta = 0.02$.

finite size of the lattice discretizing the free-hole spectrum. We pushed the limit of our computational power to consider a larger system (101^3 sites) and adopted a moderate peak broadening $\eta = 0.02$ to alleviate this problem. This allows us to find the lowest eigenenergies with sufficient precision so that the corresponding error bars are smaller than the size of the symbols. Of course, we cannot estimate the error bars due to using this version of MA, as opposed to a more sophisticated one, corresponding to a bigger variational space and thus more accurate. Nevertheless, the good qualitative agreement between these results and those obtained in the antiadiabatic limit gives us confidence that these transitions occur at lower values of Ω as well.

V. DISCUSSION

We used the MA approximation and various perturbative limits to study single polaron physics on a perovskite lattice. The main motivation was to study a multiband model with Peierls electron-phonon coupling to see if it can be mapped onto a much simpler Holstein model.

We find sharp transitions in the Peierls polaron ground-state properties. Such transitions are known to be impossible in the Holstein model [34] (more generally, any $g(\mathbf{q})$ models including Rice-Sneddon). Thus, our main conclusion is that Peierls coupling cannot automatically be replaced by simpler couplings like the Holstein model. Such a replacement could work well in the region of the parameter space where both models predict the same qualitative shape of the polaron

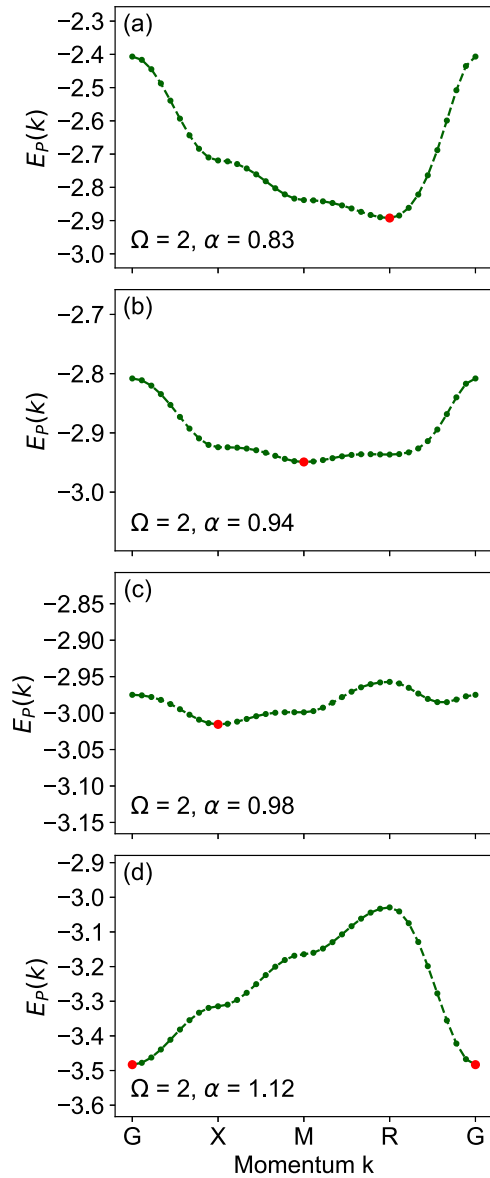


FIG. 9. Polaron dispersion calculated with MA for $t = -1$, $\Omega = 2$, $t_p = -0.2$, $\Delta = 0$ and α values as indicate on the panels. For small α we find $\mathbf{k}_{gs} = R$, see panel (a), while for large α we find $\mathbf{k}_{gs} = G$. At intermediary values, the GS (shown by the bigger red dot) is either at M or X. Other parameters and settings are like for Fig. 8.

dispersion, but will not work in the region(s) where the Peierls coupling changes the momentum of the GS. Moreover, we find that it is not enough to study a small cluster to decide whether the parameters are such that Holstein may work, one needs to study the lattice case. This is because the cluster solution suggested that mapping onto a Holstein model is good when $\Delta = t_p = 0$, whereas the lattice results demonstrate that even in this case, a sharp transition occurs with increased electron-phonon coupling.

This being said, we re-emphasize that this conclusion is valid in the insulating limit, where there is a single carrier in the system so that a single polaron forms—this limit can be studied with MA and reinforced by PT results. Unfortunately, at this time we do not have access to similarly

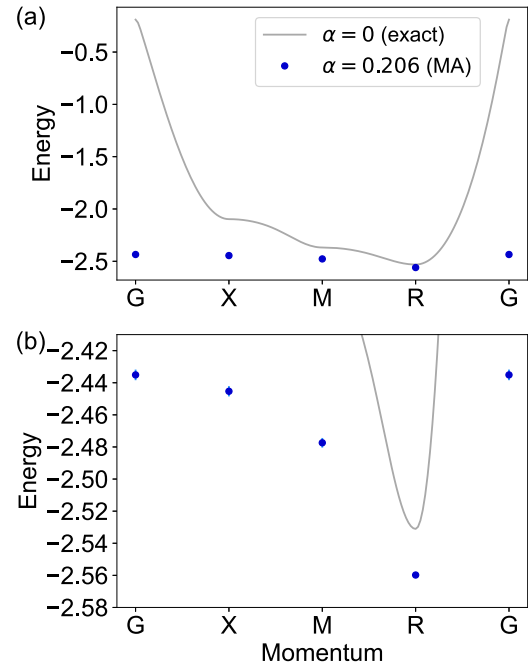


FIG. 10. Dispersion of the 3D Peierls polaron using parameters appropriate for BaBiO₃. Panel (a) shows a wider energy interval, while panel (b) focuses on the low-energy part. The gray line shows the lowest free hole band ($\alpha = 0$) while the blue symbols show the MA results (with error bars comparable to the symbol size) at the high symmetry points for a coupling $\alpha = 0.206$, for a system with 101^3 sites and $\eta = 0.02$. Other parameters are $t = -1$, $t_p = -0.3$, $\Delta = 0.19$, $\Omega = 0.033$.

accurate approximations that deal with finite concentrations of carriers, so we cannot make any confident claims about those systems. The same is true for the single polaron in the strongly adiabatic limit, where the variational space used for the MA implemented here is too limited. These questions remain open.

Keeping in mind these caveats, we now use MA to generate single polaron results for parameters appropriate for BaBiO₃ at half filling. Continuing to use $t = -1$ as our energy unit, DFT results [20] find $t_p = -0.3$, $\Delta = 0.19$, $\Omega = 0.033$, and $\alpha = 0.206$. A rough extrapolation of the curves shown in Fig. 8(b) suggests that this point falls to the left of the transition lines (the GS momentum is still at R like for the free carriers) although not by much.

Figure 10 shows the corresponding MA results at the high symmetry points, as well as the lowest free hole band (gray line). The typical error bar here is greater than that in Figs. 8 and 9, because the peak of the polaronic state is much closer to the continuum above it, and this impacts its fitting with a simple Lorentzian. The electron-phonon coupling significantly renormalizes the polaron bandwidth, proving that this is indeed a strong coupling. The GS remains at the R point like for the free hole, therefore these parameters fall in the region of the parameter space where both models predict the same qualitative shape of the polaron band. Thus, it is possible that this dispersion could be captured with an appropriately chosen Holstein model. However, to what extent this conclusion

continues to hold for the finite hole concentrations that are physically relevant for BaBiO₃ is a matter for future studies.

ACKNOWLEDGMENTS

We thank Dr. Lucian Covaci for useful discussions regarding the Chebyshev polynomial expansion. This work was supported by the Steward Blusson Quantum Matter Institute (SBQMI) and by the Natural Sciences and Engineering Research Council of Canada (NSERC).

APPENDIX A: COMPLETE HAMILTONIANS FOR THE CLUSTER MODEL

The full cluster Hamiltonian in Eq. (4) is

$$\begin{aligned} \mathcal{H} = & \Omega \sum_{i=1}^6 b_i^\dagger b_i + \Delta s^\dagger s - \sum_{i=1}^6 t(s^\dagger p_i + p_i^\dagger s) \\ & - \sum_{i=1}^6 \alpha t(s^\dagger p_i + p_i^\dagger s)(b_i^\dagger + b_i) \\ & - t_p \sum_{i=1,3,5} [(p_i^\dagger + p_{i+1}^\dagger)(p_{i+2} + p_{i+3}) + \text{H.c.}] \\ & - \beta t_p [[p_6^\dagger(b_6^\dagger + b_6) + p_5^\dagger(b_5^\dagger + b_5)](p_4 + p_3) \\ & + (p_5^\dagger + p_6^\dagger)[p_3(b_3^\dagger + b_3) + p_4(b_4^\dagger + b_4)] \\ & + [p_4^\dagger(b_4^\dagger + b_4) + p_3^\dagger(b_3^\dagger + b_3)](p_1 + p_2) \\ & + (p_4^\dagger + p_3^\dagger)[p_1(b_1^\dagger + b_1) + p_2(b_2^\dagger + b_2)] \\ & [p_1^\dagger(b_1^\dagger + b_1) + p_2^\dagger(b_2^\dagger + b_2)](p_6 + p_5) \\ & + (p_1^\dagger + p_2^\dagger)[p_6(b_6^\dagger + b_6) + p_5(b_5^\dagger + b_5)] + \text{H.c.}] \end{aligned}$$

and the full Hamiltonian in the symmetry basis in Eq. (5) is

$$\begin{aligned} \mathcal{H} = & \Omega \sum_{i=1}^6 B_i^\dagger B_i + \Delta s^\dagger s - T(s^\dagger P_1 + P_1^\dagger s) \\ & - \alpha t \sum_{i=1}^6 (s^\dagger P_i + P_i^\dagger s)(B_i^\dagger + B_i) \\ & - t_p(4P_1^\dagger P_1 - 2P_2^\dagger P_2 - 2P_3^\dagger P_3) \\ & - \beta t_p \left(\sqrt{\frac{8}{3}}(B_1^\dagger + B_1)(2P_1^\dagger P_1 - P_2^\dagger P_2 - P_3^\dagger P_3) \right. \\ & + \sqrt{\frac{2}{3}}(B_2^\dagger + B_2)(P_1^\dagger P_2 + P_2^\dagger P_1 - \sqrt{2}P_2^\dagger P_2 + \sqrt{2}P_3^\dagger P_3) \\ & + \sqrt{\frac{2}{3}}(B_3^\dagger + B_3)(P_3^\dagger(P_1 + \sqrt{2}P_2) + \text{H.c.}) \\ & + \sqrt{\frac{1}{3}}(B_4^\dagger + B_4)(P_4^\dagger(2\sqrt{2}P_1 + P_2 - \sqrt{3}P_3) + \text{H.c.}) \\ & + \sqrt{\frac{1}{3}}(B_5^\dagger + B_5)(P_5^\dagger(2\sqrt{2}P_1 + P_2 + \sqrt{3}P_3) + \text{H.c.}) \\ & \left. + \sqrt{\frac{4}{3}}(B_6^\dagger + B_6)(P_6^\dagger(\sqrt{2}P_1 - P_2) + \text{H.c.}) \right). \end{aligned}$$

APPENDIX B: DETAILS OF THE MA IMPLEMENTATION

As discussed in the main text, we implement the simplest MA⁽⁰⁾ version, which allows the phonon to appear only at one site in any given configuration. With this restriction, for $\gamma = s, x, y, z$ and $\delta = x, y, z$, we find that

$$\begin{aligned} f_{\gamma,\delta,\ell}^{(n)} = & (\tilde{f}_{\delta,\delta}^{(n+1)} + n\tilde{f}_{\delta,\delta}^{(n-1)}) [(-\alpha t)(G_{0,-\ell}^{s\gamma} + G_{0,-\ell+\delta}^{s\gamma}) \\ & + \beta t_p(\tilde{g}_{-\ell}^{\delta'\gamma} + \tilde{g}_{-\ell}^{\delta''\gamma})] \\ & + G_{0,-\ell}^{\delta\gamma} [(-\alpha t)(\tilde{f}_{s,\delta}^{(n+1)} + n\tilde{f}_{s,\delta}^{(n-1)}) \\ & + \beta t_p(\tilde{f}_{\delta',\delta}^{(n+1)} + \tilde{f}_{\delta',\delta}^{(n-1)} + n\tilde{f}_{\delta',\delta}^{(n-1)} + n\tilde{f}_{\delta'',\delta}^{(n-1)})], \end{aligned}$$

where $f \equiv f(\omega)$ while $G_0 \equiv G_0(\omega - n\Omega)$ because of the cost of the n phonons present, and then indexes γ', γ'' associated with a given γ are defined in the main text following Eq. (3). The free carrier propagators $G_0(\omega)$ are defined as:

$$\left\{ \begin{array}{l} G_{0,i-j}^{\gamma\gamma'}(\omega) \equiv \langle \gamma_i | \hat{G}_0(\omega) | \gamma_j' \rangle \\ \tilde{g}_{-\ell}^{\delta'\gamma}(\omega) \equiv G_{0,-\ell}^{\delta'\gamma}(\omega) - G_{0,-\ell-\delta'}^{\delta'\gamma}(\omega) + G_{0,-\ell+\delta}^{\delta'\gamma}(\omega) \\ \quad - G_{0,-\ell+\delta-\delta'}^{\delta'\gamma}(\omega) \\ \tilde{g}_{-\ell}^{\delta''\gamma}(\omega) \equiv G_{0,-\ell}^{\delta''\gamma}(\omega) - G_{0,-\ell-\delta''}^{\delta''\gamma}(\omega) + G_{0,-\ell+\delta}^{\delta''\gamma}(\omega) \\ \quad - G_{0,-\ell+\delta-\delta''}^{\delta''\gamma}(\omega), \end{array} \right.$$

where i, j, ℓ are site indices.

Substituting these equations of motion for $f_{\gamma,\delta,\ell}^{(n)}$ into the definitions of $\tilde{f}_{s,\gamma}^{(n)}$, $\tilde{f}_{\gamma,\gamma}^{(n)}$, $\tilde{f}_{\gamma',\gamma}^{(n)}$, and $\tilde{f}_{\gamma'',\gamma}^{(n)}$, we find that the latter define recurrence relations linking propagators with a given n only to those with $(n+1)$ and $(n-1)$. In other words, we can define a vector

$$v_{\gamma,n}^T \equiv (\tilde{f}_{s,\gamma}^{(n)}, \tilde{f}_{\gamma,\gamma}^{(n)}, \tilde{f}_{\gamma',\gamma}^{(n)}, \tilde{f}_{\gamma'',\gamma}^{(n)})^T \quad (\text{B1})$$

such that the equations of motion can be written in compact form as:

$$v_{\gamma,n} = \alpha_{\gamma n} v_{\gamma,n+1} + n\alpha_{\gamma n} v_{\gamma,n-1}. \quad (\text{B2})$$

Here $\alpha_{\gamma n}$ is a known matrix whose entries can be read directly from the equations of motion. Note that for $n=0$, after some simplifications, $v_{\gamma,0}$ can be written in terms of the various propagators $G^{\alpha\beta}(\omega)$ of interest, specifically:

$$\begin{aligned} v_{\gamma,0} = & \begin{bmatrix} (1 + e^{-ik_y a})G^{\beta s}(\omega) \\ G^{\beta\gamma}(\omega) \\ (1 - e^{ik_{\gamma'} a} + e^{-ik_{\gamma} a} - e^{i(k_{\gamma'} - k_{\gamma})a})G^{\beta\gamma'}(\omega) \\ (1 - e^{ik_{\gamma''} a} + e^{-ik_{\gamma} a} - e^{i(k_{\gamma''} - k_{\gamma})a})G^{\beta\gamma''}(\omega) \end{bmatrix} \\ = & P_{\gamma} \tilde{v}_0 \end{aligned}$$

where P_{γ} is a matrix and \tilde{v}_0 is defined to be $(G^{\beta s}, G^{\beta x}, G^{\beta y}, G^{\beta z})^T$.

Such matrix recurrence relations are solved with the ansatz $v_{\gamma,n} = A_{\gamma,n} v_{\gamma,n-1}$ which allows us to calculate the matrices $A_{\gamma,n}$ recursively, starting from $A_{\gamma,N} = 0$ for a sufficiently large N . This N defines the largest number of phonons allowed to appear in a self-energy diagram, and is increased until the results converge. Once $A_{\gamma,n=1}$ is known, the various propagators $G^{\alpha\beta}(\omega)$ are obtained from Eq. (8). Peaks in the spectral weights $-\frac{1}{\pi} \Im G^{\alpha\beta}(\omega)$ indicate the eigenenergies of \hat{H} and thus allow us to determine the lowest eigenenergy for any given momentum k .

APPENDIX C: CHEBYSHEV POLYNOMIAL EXPANSION FOR FREE PROPAGATORS

Such expansions are well established for a variety of problems. Here we briefly summarize the main steps, following Ref. [46].

Chebyshev polynomials $T_n(x) \equiv \cos(n \cos^{-1}(x))$ are well defined only for $x \in [-1, 1]$, thus we need to rescale the range of eigenvalues of the noninteracting Hamiltonian H_0 before applying the Chebyshev expansion to it. E_{\max} and E_{\min} can be found by Fourier transforming H_0 to momentum k space and maximizing or minimizing the energies in the k parameter space. We define $a = \frac{E_{\max} - E_{\min}}{2}$ and $b = \frac{E_{\max} + E_{\min}}{2}$ and write the normalized Hamiltonian as $\tilde{H}_0 = \frac{H_0 - b}{a}$ and denote the corresponding noninteracting Green's function as $\tilde{G}_0(\tilde{\omega})$, where $\tilde{\omega} = (\omega - b)/a$. We expand [46]

$$\tilde{G}_{0,j}^{\alpha\beta}(\tilde{\omega}) = \sum_{n=0}^{\infty} 2i^{-1} \frac{(\tilde{\omega} - i\sqrt{1 - \tilde{\omega}^2})^n \langle \alpha_j | T_n(\tilde{H}_0) | \beta_0 \rangle}{\sqrt{1 - \tilde{\omega}^2} (1 + \delta_{n0})}$$

where $T_0(x) = 1$, $T_1(x) = x$ and $T_{n+1}(x) = 2xT_n(x) - T_{n-1}(x)$.

If we define $|J_n\rangle \equiv T_n(\tilde{H}_0) |\beta_0\rangle$, then $|J_{n+1}\rangle = 2\tilde{H}_0 |J_n\rangle - |J_{n-1}\rangle$, thus these $|J_n\rangle$ can be determined recursively starting from $|J_0\rangle = |\beta_0\rangle$ and $|J_1\rangle = \tilde{H}_0 |\beta_0\rangle$. The summation is truncated at a value large enough so that $\tilde{G}_{0,j}^{\alpha,\beta}$ is converged. We note here that there are unphysical oscillations in the $\tilde{G}_{0,j}^{\alpha,\beta}$ obtained if plotted versus energy. This is caused by the standing waves selected due to the finite size of the system. Since η is inversely proportional to the lifetime of the state, we can either increase the size of the system or use a larger η so that the state cannot live long enough to reach the edge of the system, and hence the finite-size oscillations are smoothed out. Having a larger system would increase the demand for computational power exponentially, therefore we are forced to use a fairly large η (0.1 in our case) in order to get a smooth enough curve for $\tilde{G}_{0,j}^{\alpha,\beta}$. Rescaling back, the various free propagators are:

$G_{0,j}^{\alpha\beta}(\omega + i\eta) = \frac{1}{a} \tilde{G}_{0,j}^{\alpha\beta}(\frac{\omega - b}{a} + i\frac{\eta}{a})$ where η is the broadening of the Lorentzian peak in the energy spectrum.

APPENDIX D: DETAILS OF THE CONTINUED FRACTION SOLUTION FOR THE CLUSTER

We consider the Hamiltonian of Eq. (11), where two different electronic orbitals s and P_1 (renamed p in the following, for simplicity) are coupled to the same boson mode B_1 (renamed b in the following, for simplicity). The full Hilbert

space corresponding to the one-carrier sector is spanned by the basis $\{|s, n\rangle \equiv \frac{s^i (b^\dagger)^n |0\rangle}{\sqrt{n!}}, |p, n\rangle \equiv \frac{p^i (b^\dagger)^n |0\rangle}{\sqrt{n!}}\}$ with $n \geq 0$.

We define the propagators:

$$\begin{cases} \mathcal{S}_n(m, z) \equiv \langle s, n | \hat{G}(z) | s, m \rangle \\ \mathcal{P}_n(m, z) \equiv \langle s, n | \hat{G}(z) | p, m \rangle \end{cases}$$

Their equations of motion are generated from the appropriate expectation values of the identity $\hat{G}(z)(z - \hat{H}) = 1$. For the Hamiltonian of Eq. (11), we find:

$$\begin{aligned} \mathcal{S}_n(m, z)(z - \Delta - m\Omega) + \mathcal{P}_n(m, z)t \\ - \mathcal{P}_n(m+1, z)\alpha t \sqrt{m+1} - \mathcal{P}_n(m-1, z)\alpha t \sqrt{m} = \delta_{mn} \end{aligned}$$

and

$$\begin{aligned} \mathcal{S}_n(m, z)t - \mathcal{S}_n(m+1, z)\alpha t \sqrt{m+1} \\ - \mathcal{S}_n(m-1, z)\alpha t \sqrt{m} + \mathcal{P}_n(m, z)(z - \Omega m) = 0. \end{aligned}$$

These can be grouped as recurrence equations for 2×2 matrices:

$$\gamma_m W_{nm} - \alpha_m W_{n,m+1} - \beta_m W_{n,m-1} = \begin{bmatrix} \delta_{n,m} \\ 0 \end{bmatrix}$$

where

$$\begin{aligned} \gamma_m &\equiv \begin{bmatrix} z - \Delta - m\Omega & t \\ t & z - \Omega m \end{bmatrix}; \\ \alpha_m &\equiv \begin{bmatrix} 0 & \alpha t \sqrt{m+1} \\ \alpha t \sqrt{m+1} & 0 \end{bmatrix}; \\ \beta_m &\equiv \begin{bmatrix} 0 & \alpha t \sqrt{m} \\ \alpha t \sqrt{m} & 0 \end{bmatrix}; \\ W_{n,m} &\equiv \begin{bmatrix} \mathcal{S}_n(m, z) \\ \mathcal{P}_n(m, z) \end{bmatrix}. \end{aligned}$$

As already discussed, such recurrence relations are solved with the ansatz $W_{n,m+1} = A_{n,m+1} W_{nm}$ if $m \geq n$. This gives the continued fraction $A_{nm} = (\gamma_m - \alpha_m A_{n,m+1})^{-1} \beta_m$, which can be evaluated starting from $A_{nM} = 0$ for a sufficiently large M . Similarly, for $m \leq n$ we use the ansatz $W_{n,m-1} = B_{n,m-1} W_{n,m}$ and obtain $B_{n,m} = (\gamma_m - \beta_m B_{n,m-1})^{-1} \alpha_m$, which can be computed starting from $m = 0$, noting that $\beta_0 \equiv 0$. Putting $W_{n,n+1} = A_{n,n+1} W_{nn}$ and $W_{n,n-1} = B_{n,n-1} W_{nn}$ into the equation with $n = m$, we get:

$$W_{nn} = (\gamma_n - \alpha_n A_{n,n+1} - \beta_n B_{n,n-1})^{-1} \begin{bmatrix} 1 \\ 0 \end{bmatrix}$$

from which we can read out the propagators $\mathcal{S}_n(m, z)$ and $\mathcal{P}_n(m, z)$.

[1] L. Gao, Y. Y. Xue, F. Chen, Q. Xiong, R. L. Meng, D. Ramirez, C. W. Chu, J. H. Eggert, and H. K. Mao, *Phys. Rev. B* **50**, 4260 (1994).
[2] M. Presland, J. Tallon, R. Buckley, R. Liu, and N. Flower, *Physica C: Superconductivity* **176**, 95 (1991).
[3] J. L. Tallon, C. Bernhard, H. Shaked, R. L. Hitterman, and J. D. Jorgensen, *Phys. Rev. B* **51**, 12911 (1995).
[4] S. D. Obertelli, J. R. Cooper, and J. L. Tallon, *Phys. Rev. B* **46**, 14928 (1992).

[5] A. Subedi, O. E. Peil, and A. Georges, *Phys. Rev. B* **91**, 075128 (2015).
[6] C. M. Srivastava, N. B. Srivastava, L. N. Singh, and D. Bahadur, *J. Appl. Phys.* **105**, 093908 (2009).
[7] S. B. Abdelkhalek, N. Kallel, S. Kallel, T. Guizouarn, O. Peña, and M. Oumezzine, *Phys. B: Condens. Matter* **406**, 4060 (2011).
[8] H. Liu and X. Yang, *Ferroelectrics* **507**, 69 (2017).
[9] P. W. Anderson, *Science* **235**, 1196 (1987).

- [10] V. J. Emery, *Phys. Rev. Lett.* **58**, 2794 (1987).
- [11] M. Jiang, M. Moeller, M. Berciu, and G. A. Sawatzky, *Phys. Rev. B* **101**, 035151 (2020).
- [12] S. Johnston, A. Mukherjee, I. Elfimov, M. Berciu, and G. A. Sawatzky, *Phys. Rev. Lett.* **112**, 106404 (2014).
- [13] H. Park, A. J. Millis, and C. A. Marianetti, *Phys. Rev. Lett.* **109**, 156402 (2012).
- [14] N. Hamada, S. Massidda, A. J. Freeman, and J. Redinger, *Phys. Rev. B* **40**, 4442 (1989).
- [15] M. Shirai, N. Suzuki, and K. Motizuki, *J. Phys.: Condens. Matter* **2**, 3553 (1990).
- [16] A. I. Liechtenstein, I. I. Mazin, C. O. Rodriguez, O. Jepsen, O. K. Andersen, and M. Methfessel, *Phys. Rev. B* **44**, 5388 (1991).
- [17] K. Kunc and R. Zeyher, *Phys. Rev. B* **49**, 12216 (1994).
- [18] V. Merigliani and S. Y. Savrasov, *Phys. Rev. B* **57**, 14453 (1998).
- [19] T. Bazhurov, S. Coh, S. G. Louie, and M. L. Cohen, *Phys. Rev. B* **88**, 224509 (2013).
- [20] A. Khazraie, K. Foyevtsova, I. Elfimov, and G. A. Sawatzky, *Phys. Rev. B* **97**, 075103 (2018).
- [21] V. N. Kostur and P. B. Allen, *Phys. Rev. B* **56**, 3105 (1997).
- [22] P. B. Allen and V. N. Kostur, *Z. Phys. B: Condens. Matter* **104**, 613 (1997).
- [23] P. Piekarczyk and J. Konior, *Physica C: Superconduct.* **329**, 121 (2000).
- [24] I. B. Bischofs, V. N. Kostur, and P. B. Allen, *Phys. Rev. B* **65**, 115112 (2002).
- [25] R. Nourafkan, F. Marsiglio, and G. Kotliar, *Phys. Rev. Lett.* **109**, 017001 (2012).
- [26] T. Holstein, *Ann. Phys.* **8**, 325 (1959).
- [27] G. Seibold and E. Sigmund, *Solid State Commun.* **86**, 517 (1993).
- [28] S. Barišić, J. Labbé, and J. Friedel, *Phys. Rev. Lett.* **25**, 919 (1970).
- [29] K. Foyevtsova, A. Khazraie, I. Elfimov, and G. A. Sawatzky, *Phys. Rev. B* **91**, 121114(R) (2015).
- [30] A. Khazraie, K. Foyevtsova, I. Elfimov, and G. A. Sawatzky, *Phys. Rev. B* **98**, 205104 (2018).
- [31] W. P. Su, J. R. Schrieffer, and A. J. Heeger, *Phys. Rev. Lett.* **42**, 1698 (1979).
- [32] A. J. Heeger, S. Kivelson, J. R. Schrieffer, and W. P. Su, *Rev. Mod. Phys.* **60**, 781 (1988).
- [33] S. Li and S. Johnston, *npj Quantum Mater.* **5**, 40 (2020).
- [34] B. Gerlach and H. Löwen, *Rev. Mod. Phys.* **63**, 63 (1991).
- [35] W. Harrison, *Elementary Electronic Structure* (World Scientific, Singapore, 2004).
- [36] M. Takahashi, *J. Phys. C* **10**, 1289 (1977).
- [37] M. M. Möller and M. Berciu, *Phys. Rev. B* **93**, 035130 (2016).
- [38] M. Berciu, *Phys. Rev. Lett.* **97**, 036402 (2006).
- [39] G. L. Goodvin, M. Berciu, and G. A. Sawatzky, *Phys. Rev. B* **74**, 245104 (2006).
- [40] M. Berciu and G. L. Goodvin, *Phys. Rev. B* **76**, 165109 (2007).
- [41] O. S. Barišić, *Phys. Rev. Lett.* **98**, 209701 (2007).
- [42] M. Berciu, *Phys. Rev. Lett.* **98**, 209702 (2007).
- [43] M. M. Möller, G. A. Sawatzky, M. Franz, and M. Berciu, *Nat. Commun.* **8**, 2267 (2017).
- [44] M. Berciu, *Phys. Rev. B* **75**, 081101(R) (2007).
- [45] D. J. J. Marchand, G. De Filippis, V. Cataudella, M. Berciu, N. Nagaosa, N. V. Prokof'ev, A. S. Mishchenko, and P. C. E. Stamp, *Phys. Rev. Lett.* **105**, 266605 (2010).
- [46] A. Ferreira and E. R. Mucciolo, *Phys. Rev. Lett.* **115**, 106601 (2015).